Materials Science Forum
ISSN: 1662-9752, Vol. 1190, pp 1-9
doi:10.4028/p-besU1w
© 2026 The Author(s). Published by Trans Tech Publications Ltd, Switzerland.
Submitted: 2025-09-11
Revised: 2025-12-29
Accepted: 2026-02-28
Online: 2026-05-18

Proton Implantation–Induced Reduction of SSF Width and Associated Adverse Effects in 4H-SiC Epitaxial Layers

Kazumi Takano[1,a*], Yasuyuki Igarashi[1,b], Yohsuke Matsushita[1,c] and Takuya Morita[1,d]

[1]ITES, 1-60 Kuribayashi, Otsu, Shiga 520-2151, Japan

[a*]kazumi_takano@ites.co.jp, [b]yiga@ites.co.jp, [c]yohsuke_matsushita@ites.co.jp
[d]takuya_morita@ites.co.jp

Keywords: proton implantation, shockley-type stacking fault (SSF), photoluminescence (PL), UV irradiation.

Abstract. Proton implantation has been reported as an effective approach for suppressing bipolar degradation in 4H-SiC; however, implantation inevitably introduces lattice damage and point defects. In this work, we investigate: (i) suppression of Shockley-type stacking fault (SSF) expansion in both the proton-implanted layer and the region beyond the implanted layer, and (ii) adverse effects associated with proton implantation. Half of an n-type 4H-SiC epitaxial wafer was implanted with protons (350 keV, 1×10^{13} cm^{-2}) and annealed at 1600 °C for 30 min for dopant activation with carbon capping. SSF expansion was induced by UV laser irradiation, and photoluminescence (PL) imaging was used to quantify SSF width and observe cross sections. The proton-implanted region exhibited clearly reduced SSF expansion, with the expanded SSF width typically about 30 μm smaller than that in the non-implanted region; cross-sectional PL further confirmed that SSFs did not propagate into the near-surface implanted layer. Additional experiments with varied implantation depth and dose revealed a linear relationship between SSF width and active drift-layer thickness (defined as the drift-layer thickness minus the proton implantation depth), consistent with geometric expectations from the wafer off-cut. However, PL observations also showed anomalous SSF morphologies and evidence of dislocations, indicating that proton implantation can generate new SSF nucleation sites. Furthermore, the band-to-band PL peak intensity decreased after implantation and did not recover after the activation anneal, suggesting persistent lattice damage, including in proton-traversed regions. These results highlight a trade-off between SSF-suppression benefits and implantation-induced degradation.

Introduction

Ion implantation has long been recognized as a key technology for forming semiconductor junctions. Around 1950, R. S. Ohl and W. Shockley at Bell Telephone Laboratories patented the concept of creating junction layers using ion implantation [1,2]. In SiC (silicon carbide), in particular, p–n junction formation by thermal diffusion is extremely difficult; consequently, ion implantation is indispensable for device fabrication. Beyond junction formation, proton implantation has also been proposed as an effective means of suppressing bipolar degradation in 4H-SiC devices. Kato et al. demonstrated that bipolar degradation can be mitigated by proton implantation at doses exceeding 1×10^{12} cm^{-2}, using simple PiN diodes subjected to pulsed current stress of approximately 200 A/cm^2 [3,4]. They initially attributed the suppression mechanism mainly to the pinning of partial dislocations (PDs) by hydrogen and implantation-induced point defects, and therefore targeted proton implantation near the epitaxial/substrate interface, where basal-plane-related defects are prevalent.

Subsequent studies expanded the scope of proton implantation designs and revealed both beneficial and potentially adverse effects. Amishiro et al. fabricated SiC MOSFETs incorporating a sandwich-structured proton-implanted layer within the drift region and applied current stress of 420 A/cm^2. They reported that the width of Shockley-type stacking faults (SSFs) became slightly narrower in the region beneath the proton-implanted layer [5]. In contrast, Uchida et al. reported that proton implantation into the top 0.5 μm of the drift layer significantly increased the concentration of $Z_{1/2}$

This article is an open access article under the terms and conditions of the Creative Commons Attribution (CC BY) license
(https://creativecommons.org/licenses/by/4.0)

point defects, and that the carrier lifetime did not recover even after activation annealing [6]. These reports indicate that while proton implantation can suppress degradation-related defect evolution, it also introduces lattice damage that may persist after high-temperature annealing. Bipolar degradation in 4H-SiC is closely linked to the expansion of SSFs originating from basal plane dislocations (BPDs). Such expansion is known to proceed via recombination-enhanced dislocation glide (REDG), where the recombination energy of injected electron–hole pairs acts as the driving force for dislocation motion and SSF growth. Conventionally, SSF expansion has often been evaluated using PiN diodes under current conduction (Fig. 1), where electrons and holes are injected into the drift region. However, when the primary objective is to isolate and evaluate the effect of proton implantation itself, the expansion-visualization-contraction (EVC) method (Fig. 2) [7] provides a simpler and effective alternative: electron–hole pairs can be generated by ultraviolet irradiation without fabricating PiN structures on epitaxial substrates. A critical point in proton implantation is that lattice damage is not confined to the intended implanted layer. In the drift region, proton implantation induces defects such as $Z_{1/2}$ in the implanted layer. Moreover, when protons are implanted from the surface side, the layers traversed by protons prior to reaching the projected range are also expected to experience lattice damage. Therefore, suppression of bipolar degradation may occur not only in the implanted layer but also in these proton-traversed regions (Fig. 3). In our previous studies, degradation suppression was observed immediately after implantation and remained even after activation annealing, suggesting that persistent implantation-induced lattice damage may play a role beyond simply suppressing SSF expansion.

In this study, we investigate, using the EVC method, suppression of SSF expansion in the width direction in both the proton-implanted layer and the proton-traversed layer, and we further examine adverse effects associated with proton implantation. By correlating SSF behavior with implantation conditions and defect-related optical signatures, we aim to clarify the trade-off between SSF-suppression benefits and implantation-induced degradation.

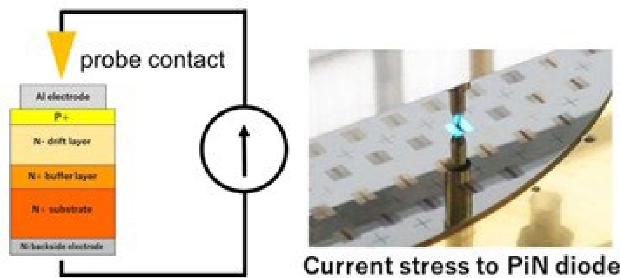

Fig. 1. Accelerated pulsed-current stress.

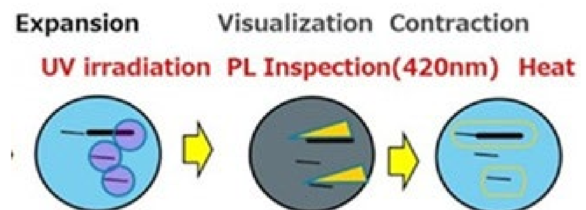

Fig. 2. EVC Screening.

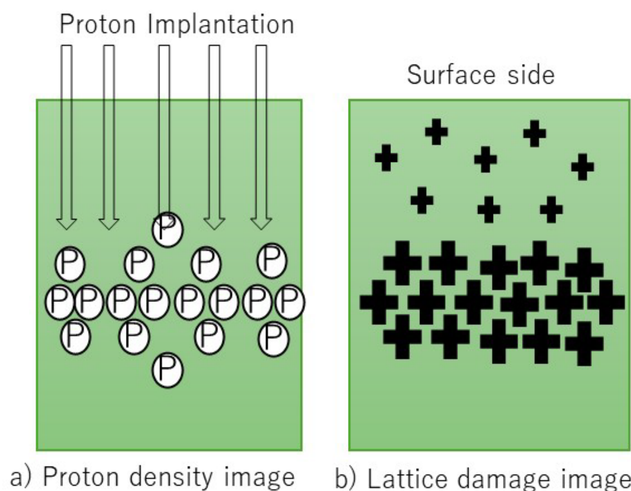

Fig. 3. Proton Implantation.

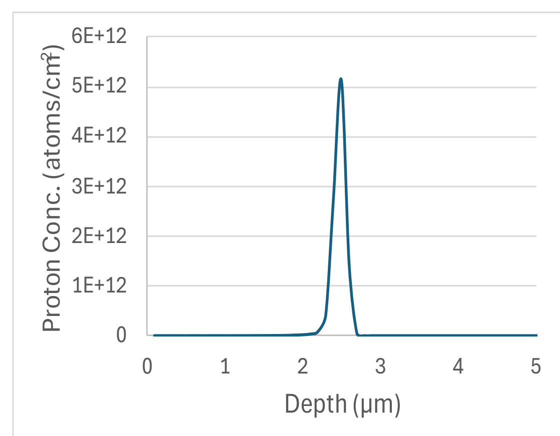

Fig. 4. Calculation result by SRIM 2013.

Experiment 1: Experimental Procedure

(1) Epitaxial wafers and proton implantation

Two commercial n-type 4H-SiC epitaxial wafers (off-cut angle: 4°) were used in this study. Epitaxial wafer A was a 100-mm-diameter 4H-SiC epi-wafer consisting of a heavily nitrogen-doped buffer layer (thickness: 1 μm; ND = 1×10^{18} cm^{-3}) and a lightly doped drift layer (thickness: 10 μm; ND = 8×10^{15} cm^{-3}). Protons were implanted into one half of the wafer surface (implantation energy: 350 keV; dose: 1×10^{13} cm^{-2}). After implantation, activation annealing was performed at 1600 °C for 30 min with carbon capping. The proton depth distribution in SiC was simulated using SRIM. The simulation indicates that the peak proton concentration is located at a depth of 2.5 μm from the incident surface, and the detailed depth profile is shown in Fig. 4.

Epitaxial wafer B was a 150-mm-diameter 4H-SiC epi-wafer with a heavily nitrogen-doped buffer layer (thickness: 3 μm; ND = 1×10^{18} cm^{-3}) and a lightly doped drift layer (thickness: 19 μm; ND = 4.5×10^{15} cm^{-3}). To clarify the relationship between SSF width and proton implantation conditions, four implantation conditions were prepared by combining two doses (1×10^{12} and 1×10^{15} cm^{-2}) and two target depths (5 μm and 15 μm). (The target depth was adjusted by decelerating protons as they passed through aluminum foil, but details remain undisclosed).

(2) UV laser irradiation for inducing SSF expansion (EVC method)

To induce SSF expansion, UV laser irradiation was performed based on the EVC method. The UV laser was the third harmonic of a YAG laser (wavelength: 355 nm; repetition rate: 50 kHz; pulse width: 20 ns). To adjust the irradiance, the beam diameter was set to 1 mm (1240 W/cm^2) and 3 mm (100 W/cm^2). The irradiation area was scanned using the following two protocols:

Protocol 1 (10×10 mm area): A linear scan at 3 mm/s with 15 μm line spacing over a 10×10 mm area for 4 h. The scanned area was centered on the boundary between the proton-implanted and unimplanted regions so that both regions were included in the same irradiation field.

Protocol 2 (four 5×5 mm areas): A linear scan at 1 mm/s with 15 μm line spacing over four non-adjacent, independent 5×5 mm areas for 3 h.

(3) Photoluminescence (PL) imaging and SSF-width measurement

Expanded SSFs were evaluated by photoluminescence (PL) imaging. An ultra-high-pressure mercury lamp was used as the excitation source. The excitation light was passed through a cut-off filter to remove wavelengths below 350 nm. PL images were acquired at an observation wavelength of 420 nm using a 1-megapixel cooled CMOS camera, providing a pixel resolution of approximately 1 μm. For the four regions irradiated under Protocol 2 (Section 2.2), the widths of ten SSFs in each region (i.e., 40 SSFs in total) were measured from the PL images to compare SSF expansion behavior among regions.

(4) Cross section sample preparation and cross-sectional PL observation

Cross section specimens were prepared from the 10×10 mm irradiation area used in Protocol 1 (Section 2.2). To investigate the depth-wise positions of the expanded SSFs, cross-sectional PL imaging was performed for two representative SSFs.

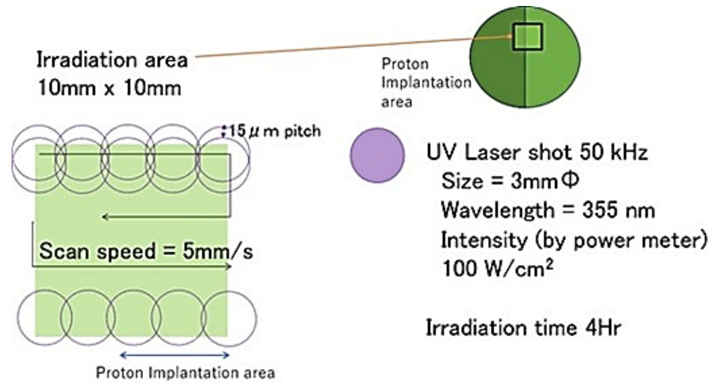

Fig. 5. Expansion by UV laser irradiation.

Result 1: Surface and Cross-Sectional PL Imaging

Fig. 6 shows PL images of a 10×10 mm² area with and without proton implantation. Fewer stripe-like features were observed in the proton-implanted region, indicating suppressed expansion of bar-shaped Shockley-type stacking faults (SSFs) in the epitaxial layer. Consistently, the expanded SSF width in the proton-implanted region was approximately 30 μm smaller than that in the non-implanted region. Cross-sectional PL imaging (Fig. 7) further confirmed that SSFs did not propagate into the near-surface layer where protons were implanted.

For statistical evaluation, a two-sample t-test was performed using the widths of 10 SSFs measured within the same 5×5 mm² area for each condition. As summarized in Table 1 and Fig. 8, a clear difference in SSF width was observed irrespective of the UV irradiance. The obtained p-values (1.03×10^{-17} and 2.56×10^{-16}) indicate that the difference is statistically significant. These results demonstrate that proton implantation yields a consistent reduction in SSF expansion, regardless of the UV irradiation dose.

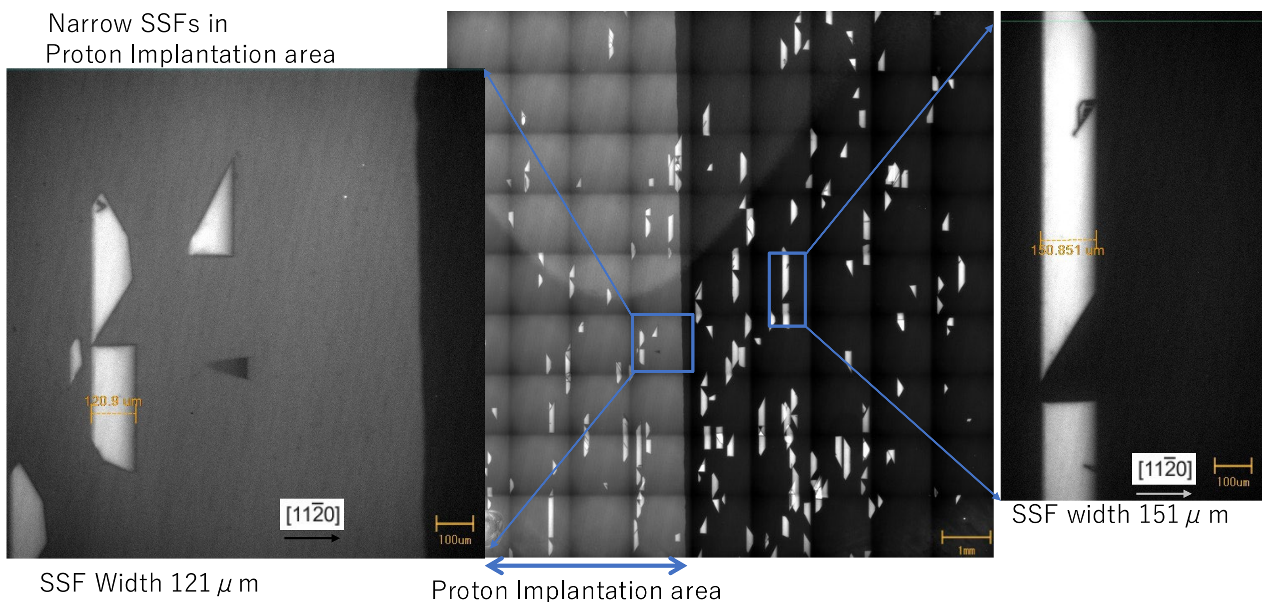

Fig. 6. PL imaging after UV irradiation.

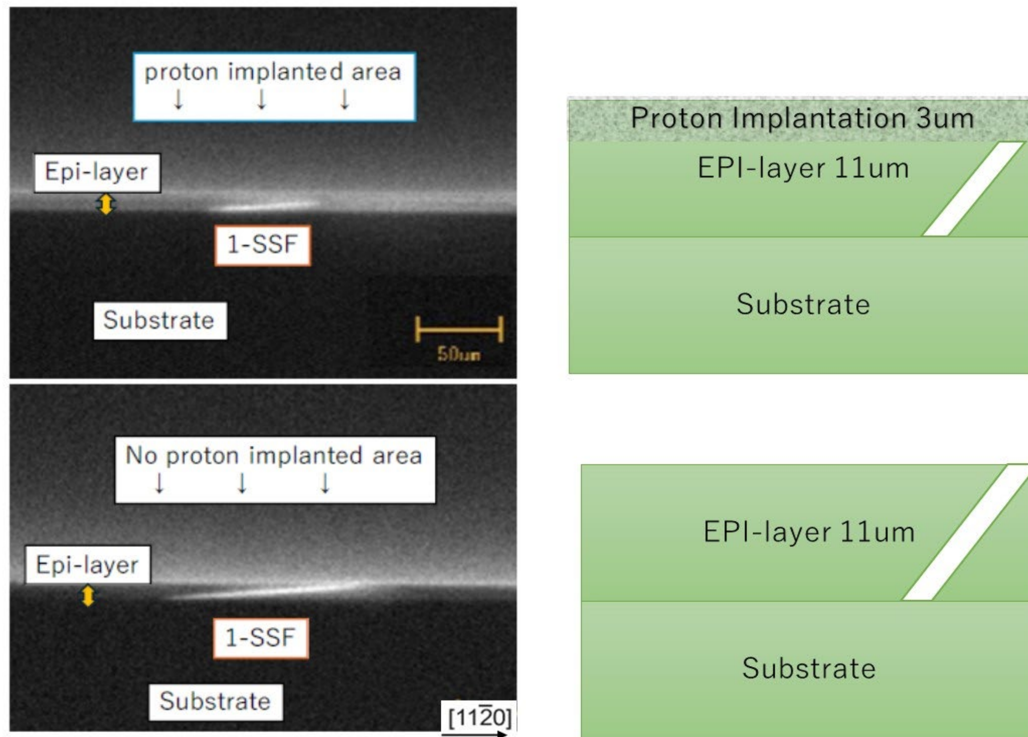

Fig. 7. Cross-section PL imaging.

Table 1. Test for the Difference of Means.

Proton	Irradiance power	Average of SSF wideth (μ m)	Standard deviation	Difference in means	P value
NO	1240W/cm^2	150.3	1.52	28.2	1.03E-17
YES	1240W/cm^2	122.1	2.17		
NO	100W/cm^2	150.1	2.08	29.5	2.56E-16
YES	100W/cm^2	120.6	2.58		

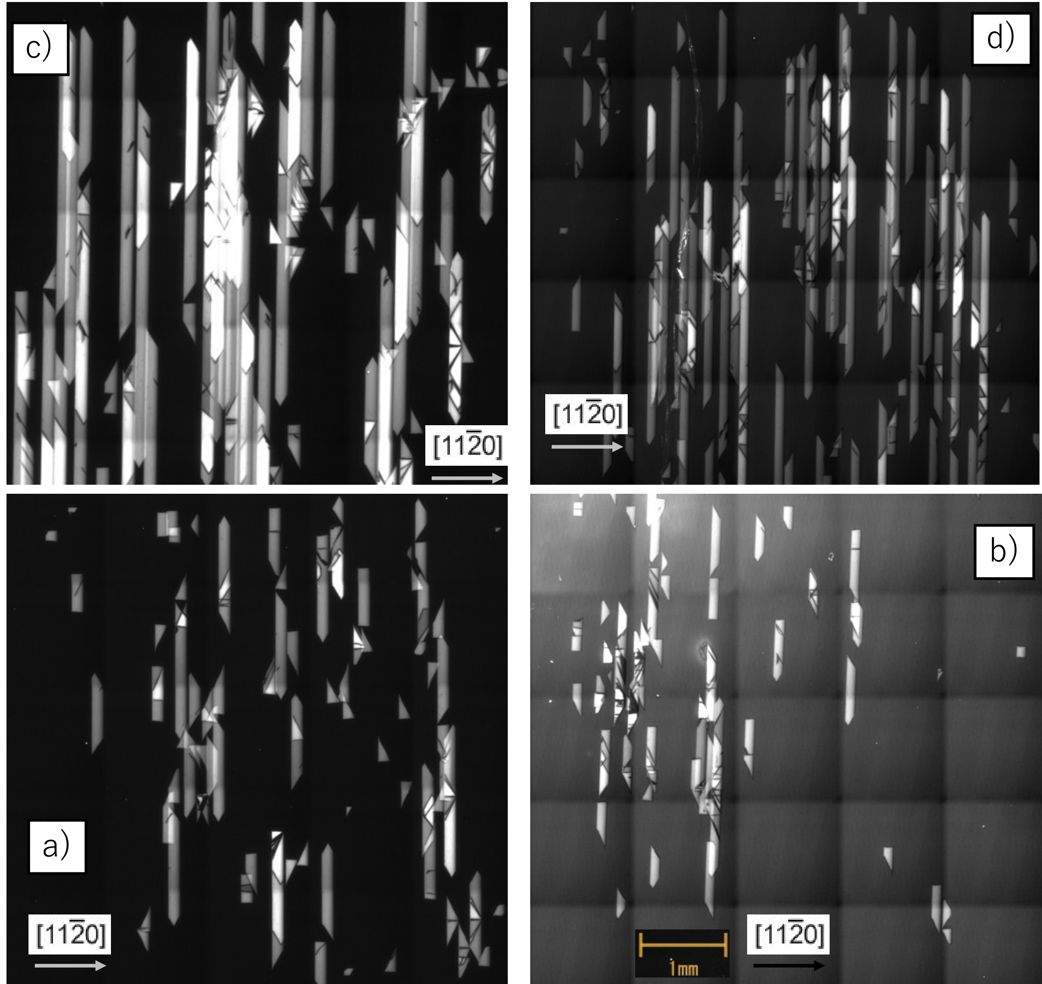

a) w/o proton, 1240 W/cm^2 1mmφ b) with proton, 1240 W/cm^2 1mmφ
c) w/o proton, 100 W/cm^2 3mmφ d) with proton, 100 W/cm^2 3mmφ

Fig. 8. PL image using BPF 420 nm.

Experiments using epitaxial wafer B showed no measurable change in SSF width at an implantation dose of 1×10^{12} cm^{-2}. At a higher dose of 1×10^{15} cm^{-2}, the band-to-band PL emission was significantly weakened, which hindered observation of the buffer layer. Although previous results indicate that SSFs can also expand into the buffer layer, the present analysis focuses on SSF expansion within the drift layer.

Fig. 9 and Table 2 plot the relationship between the active drift-layer thickness (defined as the drift-layer thickness minus the proton implantation depth) and the SSF width for wafers A and B. A clear linear correlation is observed. The extracted slope was 13.7, which is close to the theoretical value of 14.2 calculated from the 4° off-cut angle using Eq. (1).

$$\text{Width of SSF} = \text{Active drift-layer thickness} / \tan(\text{Off-cut angle}) \quad (1)$$

Table 2. Expansion Result.

	Drift layer	Proton Depth	Proton Density	Active layer	Width of SSF
wafer A	10	0	E12	10	149
		2.5	E12	7.5	107
wafer B	19	5	E15	14	200
		15	E15	4	44
	unit : μm		unit : cm^{-2}		

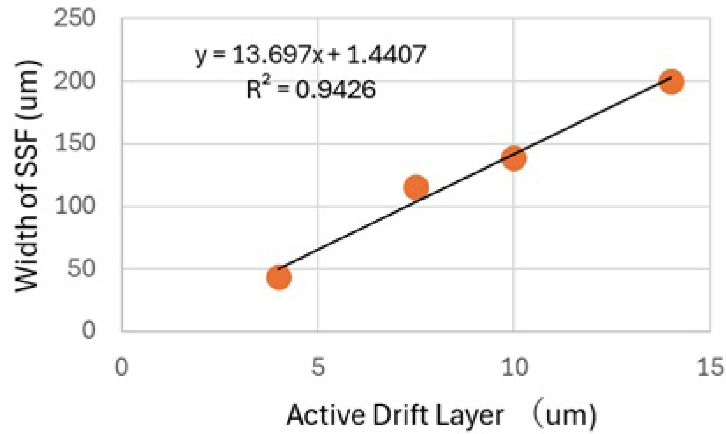

Fig. 9. Width of SSF.

Experiment and Result 2: Adverse Effect

As summarized in Table 1, the expanded SSFs in the non-implanted region showed a nearly constant width of approximately 150 μm, suggesting that SSF expansion occurred across the entire epitaxial layer. The apparent initiation points of SSF expansion were located either at the epitaxial/substrate interface or at the surface, and no initiation was observed in the middle of the epitaxial layer under the present observation conditions.

In the proton-implanted region, the SSF width was approximately 120 μm, which is comparable to the expansion length from the epitaxial/substrate interface to the lower boundary of the implanted layer. This is consistent with the notion that the implanted layer suppresses surface-initiated SSF expansion. Based on this suppression behavior, we expected that SSF expansion would predominantly originate from the epitaxial/substrate interface as shown in Fig. 10(a). However, SSFs with atypical morphologies, as exemplified in Fig. 10(b), were also observed (Fig. 11(a) yellow arrow). The SSFs observed in Fig. 8 were classified, and the results are summarized in Table 3.

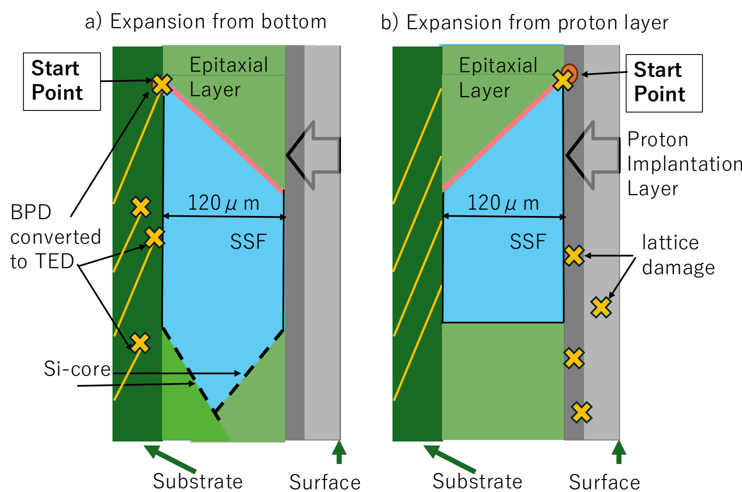

Fig. 10. Schematic Diagram of SSF.

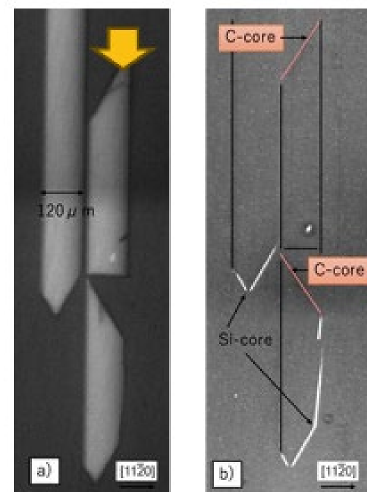

Fig. 11. PL image.

Table 3. SSF Classification.

Expansion from	Fig.8 (a)	Fig.8 (b)	Fig.8 (c)	Fig.8 (d)
Surface side	13	10	9	10
Substrate side	15	13	14	15

To further examine possible initiation sites for SSF expansion, dislocation lines were imaged at wavelengths ≥700 nm. Carbon-core dislocations, which have been reported as potential initiation sites for SSF expansion, were observed not only near the epitaxial/substrate interface but also near the lower boundary of the proton-implanted layer (Fig. 11(b)). Because prior PL observations did not show BPDs at this position, the presence of carbon-core dislocations at this depth suggests that proton implantation may have introduced or activated defect structures relevant to SSF nucleation. Although the mechanism remains unclear, these results indicate a potential adverse effect whereby implantation-induced damage could facilitate additional SSF nucleation pathways.

Discussion

The band-to-band emission peak at 390 nm in the PL spectrum is often used as a qualitative indicator of crystal quality; therefore, lattice damage introduced by ion implantation may manifest as a decrease in this peak intensity. Fig. 12 shows the PL spectra of wafer B measured before implantation, after proton implantation, and after activation annealing. After proton implantation, the band-to-band peak intensity decreased, and samples with higher doping concentrations exhibited lower peak heights (Fig. 12(a)). Fig. 12(b) presents the spectra after activation annealing; the band-to-band peak height was comparable to that measured immediately after implantation. Under the present annealing conditions, these observations suggest limited recovery of implantation-induced damage, which may be consistent with the persistence of the SSF-expansion suppression effect observed in our experiments.
In addition, as shown in Fig. 12(c), even at the same doping concentration, deeper implantation conditions were associated with lower band-to-band peak intensities. This trend suggests that residual lattice damage may extend beyond the nominal implanted layer into regions along the proton trajectory. Further investigation will be needed to determine the dominant defects responsible for the observed PL degradation.

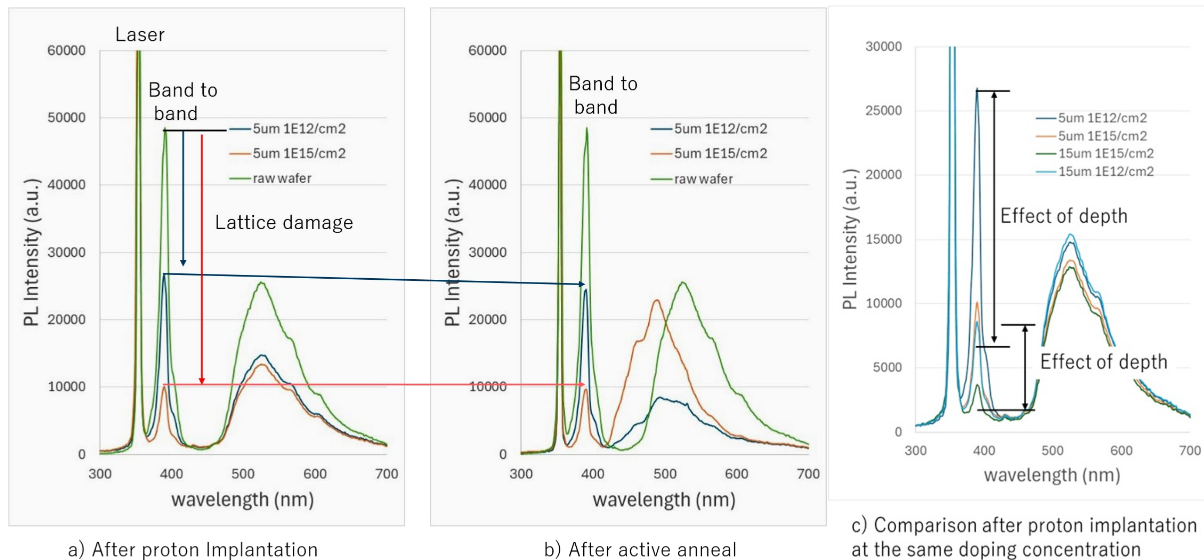

Fig. 12. PL spectrum.

In contrast, the adverse effect (the appearance of additional nucleation sites) was not clearly observed in proton-traversed regions, but was observed primarily in regions where protons are expected to stop (i.e., near the peak of the implanted proton distribution). This suggests that, within the present doping range (approximately 10^{12}–10^{15} cm^{-2}), the nature of implantation-related damage may differ between the traversed and stopping regions. In the stopping region, hydrogen can accumulate locally; if the local concentration exceeds the solubility limit, hydrogen-related voiding and/or crack-like mechanical damage (microcrack-like damage) may occur in addition to point defects. However, we did not directly confirm the presence of actual cracks in this study. Such crack-like damage can generate stress fields distinct from those associated with point defects and may

influence defect formation and SSF nucleation. Therefore, the atypical SSF morphologies and the inferred increase in nucleation sites observed in this study may reflect a combination of electronic effects from point defects and crack-like mechanical damage associated with proton stopping.

Conclusion

Using a UV-irradiation-based EVC method and PL imaging, we demonstrated that proton implantation suppresses SSF expansion in 4H-SiC epilayers. The SSF width in implanted regions was reduced (e.g., from approximately 150 μm to 120 μm in typical areas), and cross-sectional PL imaging confirmed that SSFs did not propagate into the near-surface region corresponding to the implanted layer. Moreover, the SSF width exhibited an approximately linear dependence on the effective drift-layer thickness, with a slope close to that expected from the 4° off-cut geometry. These results support the interpretation that the implanted layer acts as a barrier that limits SSF propagation.

At the same time, our observations suggest important adverse effects. The presence of atypical SSF morphologies and dislocation-related signatures indicates that proton implantation may introduce additional SSF nucleation sites, rather than solely pinning pre-existing partial dislocations. PL spectroscopy further showed that the band-to-band emission peak intensity decreased after proton implantation and remained low after activation annealing, suggesting limited recovery of implantation-induced lattice damage. The dependence on implantation depth also implies that residual damage may extend into regions traversed by protons.

Overall, proton implantation provides measurable suppression of SSF expansion, but it can also introduce persistent damage and potentially new defect-generation pathways. Therefore, optimization of implantation dose and depth, together with evaluation of both suppression efficacy and implantation-induced degradation, is essential for reliable application of this approach in 4H-SiC devices.

Acknowledgment

METI R&D Support Program for Growth Oriented Technology SMEs Grant Number JPJ005698.

References

[1] W. Shockley, US Patent 2,666,814. (1949).

[2] R.S. Ohl, US Patent 2,750,541. (1950).

[3] Masashi Kato, Ohga Watanabe, Toshiki Mii, Hitoshi Sakane, Shunta Harada, Scientific Reports 12, 18790 (2022).

[4] Shunta Harada, Toshiki Mii, Hitoshi Sakane, Masashi Kato, Scientific Reports 12, 13542 (2022).

[5] Kazuya Ishibashi, Naoki Shikama, Hiroki Niwa, Takanori Tanaka, Hiroyuki Amishiro, Akifumi Imai, Katsutoshi Sugawara, Solid State Phenomena Vol. 376, pp. 33-40, (2025).

[6] H. Uchida, M. Kobayashi, N. Hatta, S. Ishikawa, Y. Higashi, H. Sezaki, S. Harada and K. Kojima Solid State Phenomena Vol. 375, pp. 21-27, (2025).

[7] Yasuyuki Igarashi, Kazumi Takano, Yohsuke Matsushita, Chiyomi Shibata, Defect and Diffusion Forum Vol. 425, pp. 75-82, (2023).